HHS Public Access

Author manuscript

Tribol Int. Author manuscript; available in PMC 2021 May 01.

Published in final edited form as:

Tribol Int. 2020 May ; 145: . doi:10.1016/j.triboint.2020.106161.

Predicting Hydrodynamic Conditions under Worn Shoes using the Tapered-Wedge Solution of Reynolds Equation

SL Hemler[a], **DN Charbonneau**[a], **KE Beschorner**[a]

[a]Department of Bioengineering, University of Pittsburgh, 302 Benedum Hall, 3700 O'Hara Street, Pittsburgh, PA, USA

Abstract

Slips and falls are a leading cause of injuries in the workplace. The risk of slipping increases as shoe tread wears. Knowledge of the mechanics relating shoe wear to slip risk is needed to develop fall-prevention strategies. This research applies a rectangular, tapered-wedge bearing solution to worn shoes and compares the results to experimentally measured under-shoe fluid pressure results. Changes in the size of the shoe outsole worn region and fluid dispersion capabilities were recorded for four, slip-resistant shoes which were systematically abraded. The film thickness predicted by the solution correlated well with the measured force supported by the fluid. The results provide support that the tapered-wedge solution can be used to assess slip risk in worn shoes.

Keywords

mixed lubrication; fluid dynamics; slips & falls; shoe wear

1. Introduction

Slips and falls account for a large portion of non-fatal, occupational injuries. These slips often occur due to a lack of friction at the shoe-floor interface in the presence of a liquid lubricant [1, 2]. Research has shown that as shoes become worn, the coefficient of friction between the shoe and flooring in the presence of high viscosity fluids decreases [3, 4] due to a reduced capacity of the tread to disperse fluid [3–6]. Therefore, understanding the effects of shoe tread geometry and wear on under-shoe hydrodynamics is important for reducing slip risk.

Corresponding Author: Kurt E. Beschorner – BESCHORN@pitt.edu.

CRediT Author Statement

Sarah L. Hemler: Conceptualization, Methodology, Formal analysis, Writing-original draft, Writing-review & editing, Visualization

Danielle N. Charbonneau: Methodology, Writing-review and editing

Kurt E. Beschorner: Conceptualization, Methodology, Writing-review and editing, Supervision, Project administration, Funding acquisition

Competing Interest

The authors have no competing interests with the work described in this manuscript.

Shoe friction performance is dependent on the outsole geometry. Previous studies have identified tread parameters (size, orientation, depth, contact area) that affect traction performance [7–10]. The effects of material thickness ratios, resultant rubber tread block stiffness, and surface roughness on the friction coefficient have also been explored [10, 11]. Shoes marked as 'slip-resistant' (SR) by manufacturers have tread pattern designs that tend to have smaller tread blocks separated by tread channels. These channels allow for fluid dispersion that ameliorate under-shoe hydrodynamic pressures [12]. However, research on predicting changes to under-shoe fluid dispersion based on the tread loss is still emerging.

Mechanics models have emerged as an important tool for understanding shoe-floor friction mechanics and predicting the influence of footwear on shoe-floor friction. These models can be broadly categorized as contact friction models and thin-film fluid models. The contact friction models have used finite element analysis to predict hysteresis friction [13–15] and applied beam mechanics to determine the influence of tread bending stiffness on contact area [9, 10] and slipping [16]. Shoe-floor hydrodynamic models have typically applied Reynolds equation (or derivations based on this equation) to shoe-floor contaminant interactions [17, 18]. Of these two hydrodynamic modeling efforts, one modeled the shoe tread as a single rough hemisphere [17]. Proctor and Coleman modeled the entire shoe based on the tapered wedge solution of Reynolds equation [18]. This model, however, was not validated against experimental data and was primarily focused on the effects of floor roughness on shoe-floor friction. Thus, further development of a shoe-floor hydrodynamics solution may yield additional insight into the influence of shoe geometry on shoe-floor-contaminant interactions.

Recently, under-shoe fluid pressures and the friction coefficient have been experimentally measured for progressive shoe wear [3]. These measurements may offer an opportunity to validate under-shoe hydrodynamics solutions (such as the one suggested by Proctor and Coleman). Past experiments have demonstrated that under-shoe fluid pressures are sensitive to the size of the worn region consistent with the predictions of thrust bearing models [18]. However, fluid dynamics models of shoe-floor interactions based on geometrical features of the worn condition have not yet been compared to experimental measurements of under-shoe hydrodynamic conditions.

The purpose of this study is to evaluate the relationship between film thickness prediction based on a rectangular, tapered-wedge bearing solution and experimentally measured fluid hydrodynamics across shoes with simulated wear.

2. Materials & Methods

This study represents a post-hoc analysis of data that has been previously reported [3, 13]. Specifically, this study applies the tapered wedge solution of Reynolds equation (modeling) to relate the measured size of the worn region to the measured under-shoe fluid load support (experimental). An iterative experimental procedure was performed that alternated between: 1) abrading of shoe outsoles; and 2) testing coefficient of friction, under-shoe fluid pressures, and tread volume loss (Figure 1; adapted from [3]). Previously, we have reported changes in friction performance and under-shoe fluid hydrodynamics

during wear progression [3]. Furthermore, we have reported a finite element model that predicted changes in tread geometry due to wear [13]. Given these previous reports, the methodological details are only briefly described.

2.1. Abrasion Protocol

Five shoes labeled as slip-resistant shoes were used in this study (Figure 2; adapted from [3]). The right shoe of each pair was mechanically abraded at three different shoe orientations (17°, 7°, 2°). The angles were chosen to reflect the orientation of the shoe during walking from heel strike to flat foot [19]. One of the five shoes was excluded from this analysis since two distinct worn regions were observed in the middle of the heel compared to a single worn region at the rear of the heel that was observed for the other shoes. To wear the shoes, abrasive paper (18μm diameter particles) was slid across each shoe at 9.65 m/s for 20 seconds at each of the three angles. The normal force was ~40 N. Abrasive grease was used to reduce heat buildup and was cleaned from the shoes before friction testing. The shoes were progressively worn using this protocol. The number of wear iterations ranged from 13 to 35.

2.2. Mechanical Shoe Testing Protocol

Prior to wear and after each wear cycle, the shoes were slid across a contaminated floor surface that simulated a slipping action using a robotic device as seen in a previous study [3]. The robotic slip tester measured ground reaction forces and under-shoe fluid pressures. The fluid pressure sensors each had an inlet diameter of 3.2 mm and were recessed beneath the floor surface.

The shoes, attached to a shoe last, were slid across a vinyl composite tile (Armstrong, 51804; Rq = 3.13±0.42 μm) covered with a diluted glycerol solution (90% glycerol, 10% water by volume; 219 cP). Sliding conditions that are valid predictors of slipping and consistent with the shoe at the onset of slipping were used (shoe angle of 17° [20, 21], sliding speed of 0.3 m/s [20–22], and normal force of 250 N [23, 24]). Twenty fluid pressure scans were collected at 5 mm intervals to estimate under-shoe fluid pressures.

At baseline and after each wear cycle, the heel tread geometry was recorded by creating a silicone rubber mold of the shoe heel as reported in a previous study [3]. Using this mold, the size of the worn region was measured for each shoe heel outsole at baseline and after each wear cycle. This metric was defined as the product of the longest and widest continuous area without tread channels. The length (l) was measured along the long axis of the foot (anterior to posterior) and the width (b) was measured perpendicular to the long axis (medial to lateral).

3. Theory & Calculations

3.1. Data Analysis

The average friction coefficient across the five trials per wear cycle was calculated from the ground reaction forces. Fluid pressure sensor data that were five standard deviations above the baseline levels were included in the analysis [3, 12]. Numerical integration was

performed to calculate the fluid force (i.e., load supported by the fluid) based on the fluid pressure at the ith frame (p_i), perpendicular distance between scans (Δx 5 mm), the sliding velocity (u = 0.3 m/s), and the time between each frame (Δt = 2 ms) (Eq. 1) [6]. Fluid force across the twenty scans (4 scans per trial * 5 trials) was summed.

$$F_{fluid} = \sum p_i \, \Delta x \, \Delta y = \sum p_i \, \Delta x \, u \, \Delta t \tag{1}$$

3.2. Fluid Film Calculations

The tapered-wedge solution by Fuller, which was later applied to shoes by Proctor and Coleman, was used to relate hydrodynamic theory to the shoe-floor contaminant interface [18, 25]. In the solution, the minimum film thickness, h_0, occurs at the rear edge of the wedge [25]. As such, the predicted film thickness (PFT) applies to the rear edge of the worn heel. The predicted film thickness (PFT) was calculated as a function of dynamic viscosity (μ = 214 cP), the sliding speed ($u = 0.3\frac{m}{s}$), length of the wedge (l), width of the wedge (b), normal force applied to the wedge (F = 250 N), and K_p, a factor calculated from the incline of the wedge [25] (Eq. 2). An average K_p value of 0.025 was used to simplify the calculations [25].

$$h_0 = \sqrt{\frac{6\mu u l^2 b}{F} * K_p} \tag{2}$$

This equation was adapted to allow for side leakage since the shoes contained no border to prevent leakage. Thus, the factor, η, was added as a correction factor related to the ratio of the width over the length of the wedge [25]. The factor, η, is dependent on the bearing dimensions (i.e., geometry of the region of the shoe without tread) and was calculated for each shoe and wear cycle. Therefore, η, and thus PFT values were calculated for each wear cycle, j (Eq. 3).

$$h_{0_j} = \sqrt{\frac{6\mu u l_j^2 b_j \eta_j K_p}{F}} \tag{3}$$

3.3. Statistical Analysis

To quantify the relationship between the PFT and the fluid force, ANOVA methods were used. Specifically, the dependent variable was the experimentally-measured fluid force and the independent variables were shoe, PFT, and their interaction. To normalize residuals of the fluid force data and satisfy the assumptions of the statistical model, a square root transformation was used. When the size of the worn region did not change between wear cycles, only the first data point was used until the worn region increased.

4. Results

In the experiment, the fluid force values ranged from 0 to 97.4 N and the friction coefficient ranged from 0.057 to 0.41. Applying the size of the worn region to the tapered-wedge solution model, the PFT values ranged from 0.6 to 42 μm with an average film thickness of 18.7±11.6 μm. An increase in fluid force was associated with an increase in PFT (Figure 3; $F_{1,71} = 462.1$, $p < .001$). Fluid force was influenced by shoe type ($F_{3,71} = 45.7$, $p < .001$). The fluid force was not affected by the interaction of the PFT and the shoe type ($F_{3,71} = 2.2$, $p = .098$).

5. Discussion

In this study, the tapered-wedge model of film thickness was predictive of the experimentally-measured fluid force. An increase in fluid force coincided with an increase in PFT, which was based on size of the worn region and testing parameters. This relationship was seen regardless of shoe tread type for all SR shoes. As such, calculating film thickness based on geometric measures and fluid viscosity may be feasible for predicting the fluid dispersion capabilities of shoe tread.

The PFT values reasonably predicted the lubrication regime of the shoe-floor-liquid system which has been shown to be sensitive to shoe wear [3]. The lubrication regime is often described using the lambda ratio (λ) which is the minimum film thickness normalized to the composite RMS surface roughness (R_q) (Eq. 4) [26]. When $\lambda < 1$, the surfaces are acting in the boundary lubrication regime where friction is dominated by contacting asperities. As lambda increases, friction decreases as the interaction transitions to the mixed lubrication regime ($1 < \lambda < 5$), and then moves into the hydrodynamic lubrication regime ($\lambda > 5$) or the elasto-hydrodynamic lubrication regime ($3 < \lambda < 10$). In this study, the fluid force started to increase when $\lambda \approx 1$ ($h_{\lambda=1}$=3.5±0.2). Thus, this simple model yields predictors in line with the experimentally observed transition from boundary to mixed lubrication. The friction coefficient decreased as the shoes became more worn. The increase in wear led to an increase in the lambda ratio and PFT values, implying a shift from the boundary lubrication regime to the mixed lubrication. (Figure 4).

$$\lambda = \frac{h_0}{\sqrt{{R_{q_{floor}}}^2 + {R_{q_{shoe}}}^2}} \tag{4}$$

Simple modeling approaches may be useful for predicting under-shoe hydrodynamics even when more sophisticated approaches are available. Previous models have explored fluid dynamics and wear using sophisticated models. For example, Beschorner, et al. developed a mixed-lubrication model using a pin-on-disk apparatus based on Hertzian contact mechanics and Reynolds equation for understanding how shoe-floor friction changes with varying speed and shoe material changes [17]. Moghaddam et al., demonstrated the use of finite element analysis in modeling shoe wear progression [13]. These previous modeling efforts required iterative methods and complex solution techniques (finite difference method and finite element modeling, respectively) that might be inaccessible to non-engineering users.

However, the method presented by Proctor and Coleman which is also utilized in the present study uses simpler methods to predict under-shoe hydrodynamic effects based on a reasonably simple equation (Eq. 2) and a few simple geometric measurements of the tread's worn region [18]. Importantly, this model was valid in its predictions despite its simplicity. The practicality and simplicity of the model presented in this study may enable it to be employed by a wide audience.

This solution can be used as a pragmatic tool for determining slip risk based on shoe geometry. Interestingly, the prediction of fluid force via film thickness (R^2=0.66) in this study was stronger compared to the prediction of fluid force based on wear sliding distance (R^2=0.38) as seen in Figure 5 and further explored in a previous study [3]. Thus, the actual shoe geometry acts as a better predictor of shoe wear and subsequent slip risk compared to the amount of usage. Practically, this is an important consideration for determining slip risk thresholds for shoe wear. Previous studies have focused primarily on time of wear as a metric for replacing shoe wear [27]. However, the shoe outsole geometry, specifically the size of the worn region, may be a better indicator of under-shoe hydrodynamics and thus, slip risk, as supported by this study and a previous study [3].

Certain study limitations and future directions should be noted. Only one flooring, and contaminant are utilized. Previous research has shown that under-shoe fluid pressures are sensitive to these metrics [28–30]. Thus, futures studies may consider expanding upon the work in this study to contaminants with varying material parameters (viscosity, shoe materials) that encompass an array of materials used in industrial settings. Validating this model with naturally-worn shoes and for human slips would increase confidence in its relevance to walking and slipping. Furthermore, comparing the model predictions to experimentally-measured film thickness values (e.g., using ultrasound methods [31]) may provide additional detail regarding the ability of this model to assess shoe-floor hydrodynamic conditions. Thus, important opportunities exist to further our understanding on how to apply the tapered wedge model to worn shoes.

6. Conclusion

Determining the influence of shoe tread wear on slip risk is a key factor in the design of safe and durable shoe tread for the workplace. The tapered wedge solution is a good start for understanding the relationship between wear and under-shoe hydrodynamics. Furthermore, this model may be useful for determining wear thresholds for particular shoe, floor, and liquid material properties to reduce slipping events.

Acknowledgements

This study was funded by grants from the National Institute for Occupational Safety & Health (NIOSH R01 OH 010940–01), the National Science Foundation (NSF GRFP 1747452), and the National Institute of Arthritis and Musculoskeletal and Skin Diseases (R43AR064111).

Abbreviations

η	wedge correction factor

$\boldsymbol{\lambda}$	lambda ratio (h_0/R_q)
$\boldsymbol{\mu}$	dynamic viscosity
$\boldsymbol{\Delta t}$	time between samples
$\boldsymbol{\Delta x}$	perpendicular distance between fluid pressure scans
b	width of wedge
$\boldsymbol{h_0}$	minimum film thickness
l	length of wedge
u	sliding velocity
PFT $\equiv \boldsymbol{h_0}$	predicted film thickness
$\boldsymbol{p_i}$	fluid pressure
F	normal force
$\mathbf{K_p}$	wedge incline factor
$\mathbf{R_q}$	composite RMS surface roughness

8. References

1. Burnfield JM and Powers CM, Prediction of slips: an evaluation of utilized coefficient of friction and available slip resistance. Ergonomics, 2006. 49(10): p. 982–995. [PubMed: 16803728]
2. Hanson JP, Redfern MS, and Mazumdar M, Predicting slips and falls considering required and available friction. Ergonomics, 1999. 42(12): p. 1619–1633. [PubMed: 10643404]
3. Hemler SL, et al. , Changes in under-shoe traction and fluid drainage for progressively worn shoe tread. Applied Ergonomics, 2019. 80: p. 35–42. [PubMed: 31280808]
4. Grönqvist R, Mechanisms of friction and assessment of slip resistance of new and used footwear soles on contaminated floors. Ergonomics, 1995. 38(2): p. 224–241. [PubMed: 28084937]
5. Beschorner KE, Albert DL, and Redfern MS, Required coefficient of friction during level walking is predictive of slipping. Gait & posture, 2016. 48: p. 256–260. [PubMed: 27367937]
6. Singh G and Beschorner KE, A Method for Measuring Fluid Pressures in the Shoe–Floor–Fluid Interface: Application to Shoe Tread Evaluation. IIE Transactions on Occupational Ergonomics and Human Factors, 2014. 2(2): p. 53–59. [PubMed: 31106007]
7. Li KW and Chen CJ, The effect of shoe soling tread groove width on the coefficient of friction with different sole materials, floors, and contaminants. Applied ergonomics, 2004. 35(6): p. 499–507. [PubMed: 15374757]
8. Li KW, Wu HH, and Lin Y-C, The effect of shoe sole tread groove depth on the friction coefficient with different tread groove widths, floors and contaminants. Applied Ergonomics, 2006. 37(6): p. 743–748. [PubMed: 16427022]
9. Yamaguchi T, Katsurashima Y, and Hokkirigawa K, Effect of rubber block height and orientation on the coefficients of friction against smooth steel surface lubricated with glycerol solution. Tribology International, 2017. 110: p. 96–102.
10. Moriyasu K, et al. , Friction control of a resin foam/rubber laminated block material. Tribology International, 2019. 136: p. 548–555.
11. Ido T, et al. , Sliding friction characteristics of styrene butadiene rubbers with varied surface roughness under water lubrication. Tribology International, 2019. 133: p. 230–235.

12. Beschorner KE, et al. , Fluid pressures at the shoe–floor–contaminant interface during slips: Effects of tread & implications on slip severity. Journal of biomechanics, 2014. 47(2): p. 458–463. [PubMed: 24267270]
13. Moghaddam SRM, et al. , Computational Model of Shoe Wear Progression: Comparison with Experimental Results. Wear, 2019.
14. Moghaddam SRM, et al. , Predictive multiscale computational model of shoe-floor coefficient of friction. Journal of biomechanics, 2018. 66: p. 145–152. [PubMed: 29183657]
15. Moghaddam SRM, Iraqi A, and Beschorner KE, Finite Element Model of Wear Progression in Shoe Soles, in STLE Tribology Frontiers Conference. 2014: Chicago.
16. Trkov M, et al. , Shoe–floor interactions in human walking with slips: Modeling and experiments. Journal of biomechanical engineering, 2018. 140(3): p. 031005.
17. Beschorner KE, et al. , Modeling mixed-lubrication of a shoe-floor interface applied to a pin-ondisk apparatus. Tribology Transactions, 2009. 52(4): p. 560–568.
18. Proctor TD and Coleman V, Slipping, tripping and falling accidents in Great Britain—present and future. Journal of Occupational Accidents, 1988. 9(4): p. 269–285.
19. Kadaba MP, Ramakrishnan H, and Wootten M, Measurement of lower extremity kinematics during level walking. Journal of orthopaedic research, 1990. 8(3): p. 383–392. [PubMed: 2324857]
20. Albert DL, Moyer BE, and Beschorner KE, Three-Dimensional Shoe Kinematics During Unexpected Slips: Implications for Shoe–Floor Friction Testing. IISE Transactions on Occupational Ergonomics and Human Factors, 2017. 5(1): p. 1–11.
21. Iraqi A, et al. , Coefficient of friction testing parameters influence the prediction of human slips. Applied ergonomics, 2018. 70: p. 118–126. [PubMed: 29866300]
22. ASTM, American Society for Testing and Materials, ASTM F2913–11: Standard Test method for Measuring the Coefficient of Friction for Evaluation of Slip performance of Footwear and Test Surfaces/Flooring Using a Whole Shoe Tester. 2011, ASTM International: West Conshohocken, PA.
23. Iraqi A and Beschorner KE. Vertical Ground Reaction Forces During Unexpected Human Slips. in Proceedings of the Human Factors and Ergonomics Society Annual Meeting. 2017. SAGE Publications Sage CA: Los Angeles, CA.
24. Iraqi A, et al. , Kinematics and kinetics of the shoe during human slips. Journal of biomechanics, 2018. 74: p. 57–63. [PubMed: 29759653]
25. Fuller D, Theory and Practice of Lubrication for Engineers. 1956, New York: John Wiley & Sons, Inc.
26. Stachowiak G and Batchelor AW, Engineering Tribology. 2013, Oxford, UNITED STATES: Elsevier Science & Technology.
27. Verma SK, et al. , Duration of slip-resistant shoe usage and the rate of slipping in limitedservice restaurants: results from a prospective and crossover study. Ergonomics, 2014. 57(12): p. 1919–1926. [PubMed: 25205136]
28. Beschorner KE, et al. , Effects of slip testing parameters on measured coefficient of friction. Applied ergonomics, 2007. 38(6): p. 773–780. [PubMed: 17196925]
29. Chanda A, Jones TG, and Beschorner KE, Generalizability of Footwear Traction Performance across Flooring and Contaminant Conditions. IISE Transactions on Occupational Ergonomics and Human Factors, 2018(just-accepted): p. 1–23.
30. Chanda A, Reuter A, and Beschorner KE, Vinyl Composite Tile Surrogate for Mechanical Slip Testing. IISE Transactions on Occupational Ergonomics and Human Factors, 2019. 7(2): p. 132–141. [PubMed: 32724872]
31. Dwyer-Joyce R, Drinkwater B, and Donohoe C, The measurement of lubricant–film thickness using ultrasound. Proceedings of the Royal Society of London. Series A: Mathematical, Physical and Engineering Sciences, 2003. 459(2032): p. 957–976.

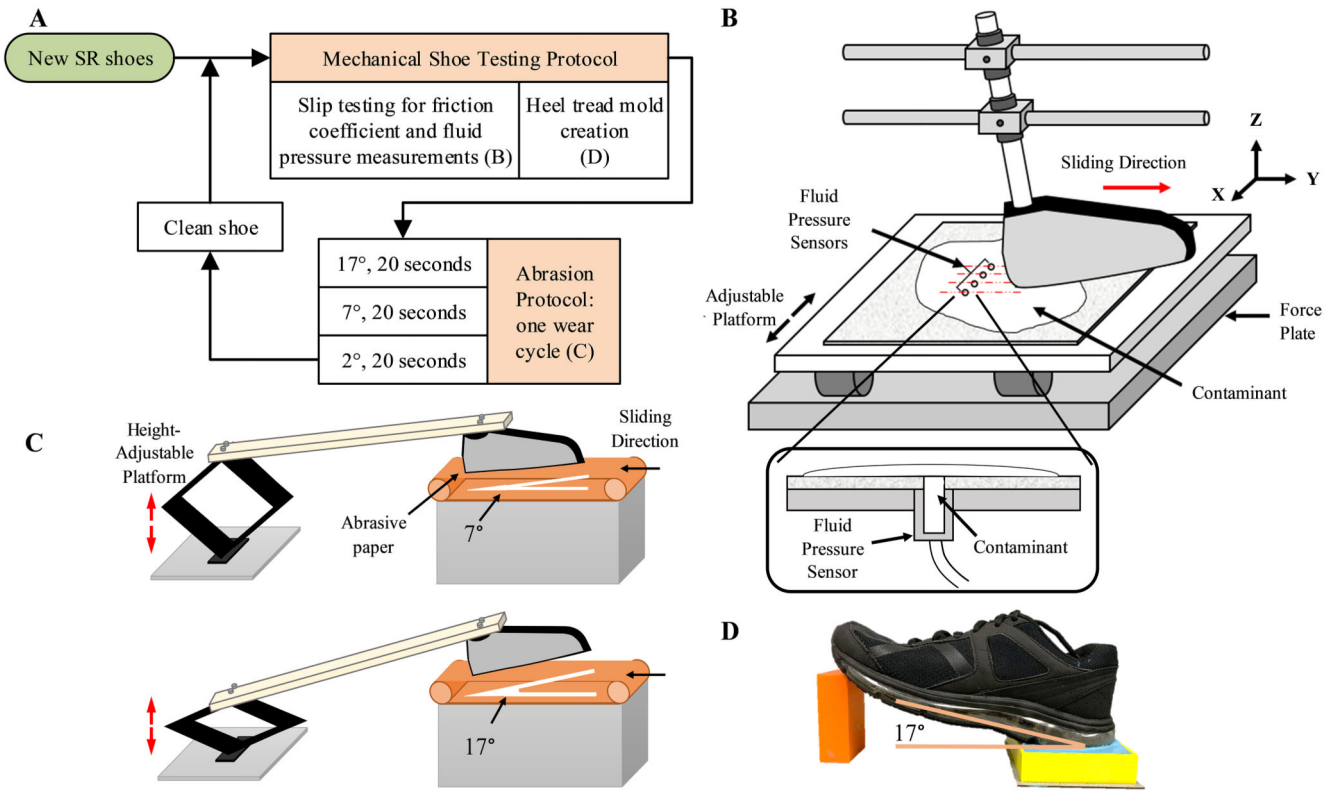

Figure 1.

A) Flow diagram of mechanical shoe testing protocol and abrasion protocol. B) A robotic slip tester was used to slid each shoe across a contaminated surface along the Y-axis with four fluid pressure sensors. The adjustable platform was moved 5 mm in the X-direction after each trial. A cross-sectional view of the fluid pressure sensor is shown. C) The abrasion protocol consisted of wearing down the shoes on abrasive paper at three angles for 20 seconds each. Examples of wear at 7° and 17° are presented. D) Molds of the heel tread were created at baseline and after each wear cycle at a 17° sagittal plane angle. Figure adapted from [3].

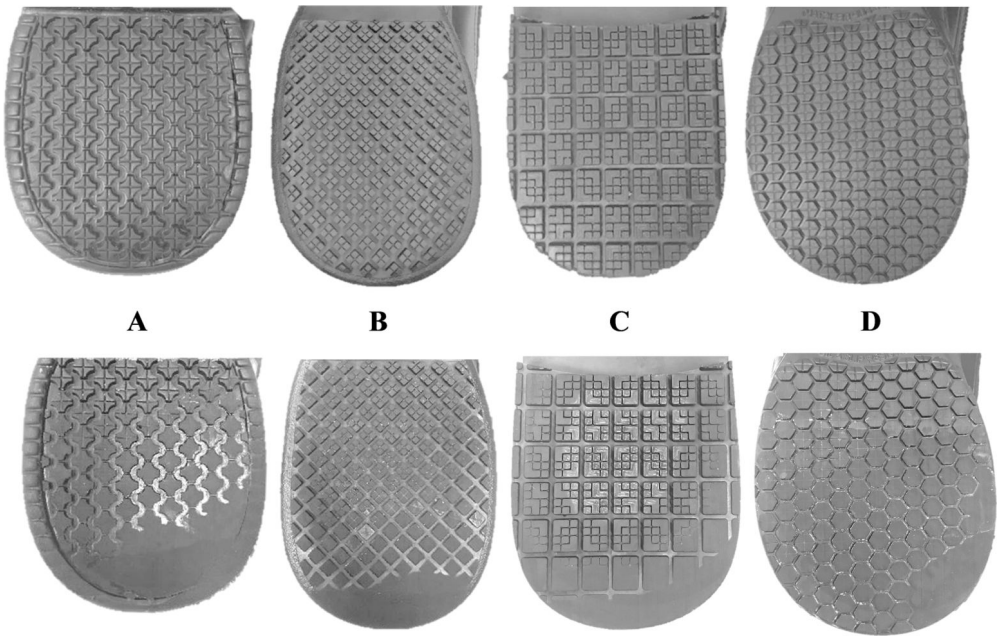

Figure 2.
The heel of the four shoes mechanically abraded at baseline (top) and after the last wear cycle (bottom).

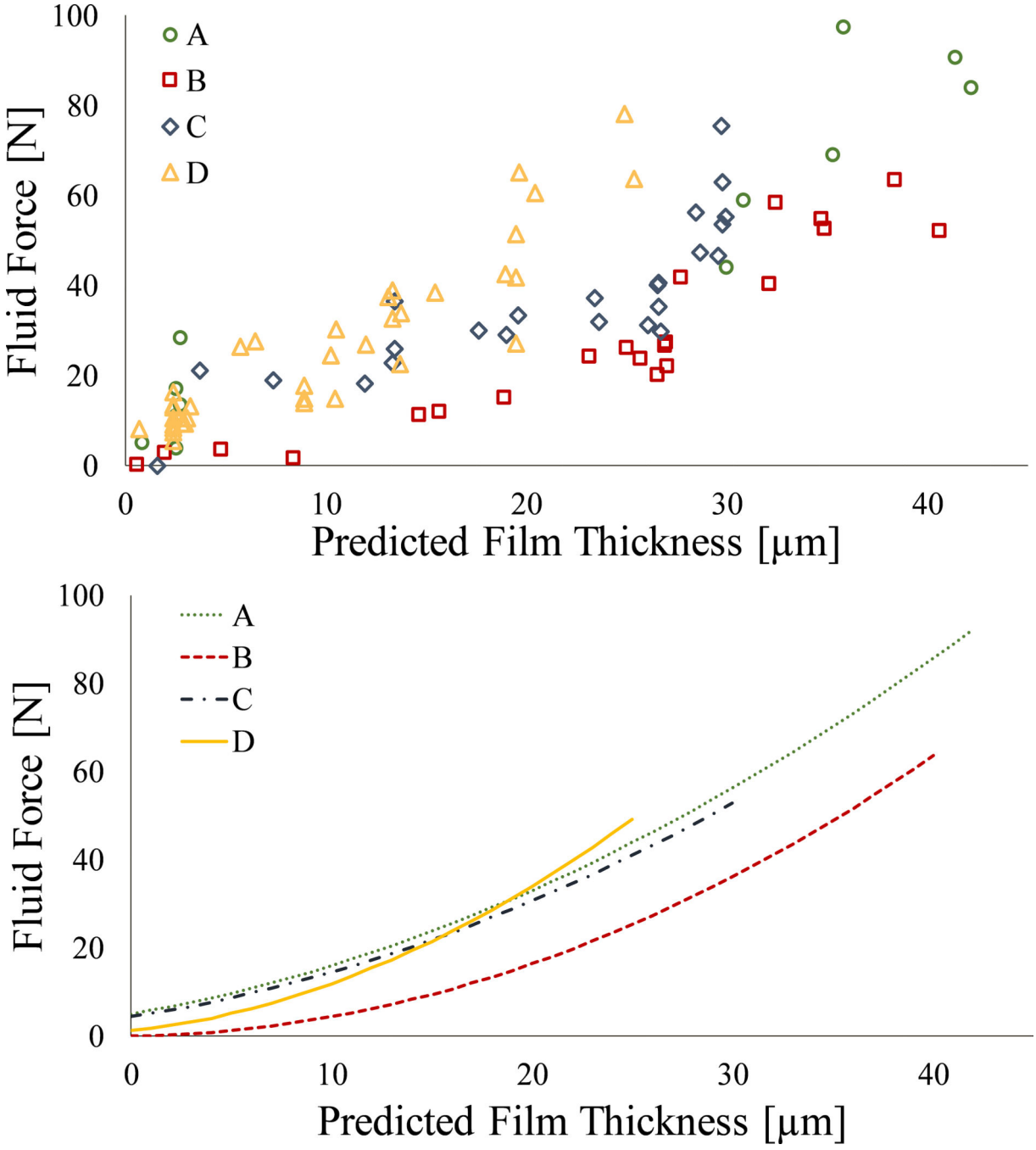

Figure 3.
(Top) Experimentally-measured fluid force with respect to the PFT for the shoes A-D. (Bottom) Regression lines for fluid force and PFT relationship for each shoe based on statistical analysis.

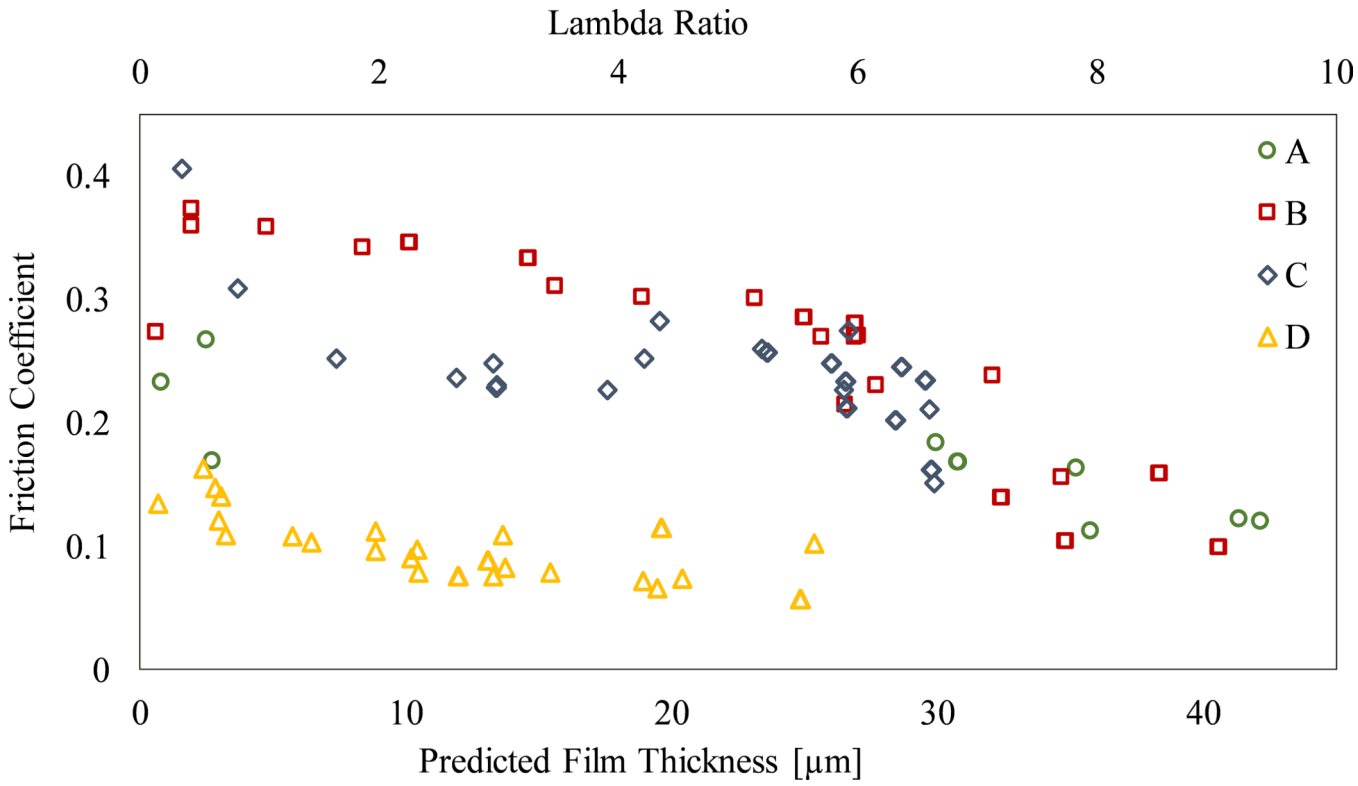

Figure 4.

The friction coefficient with respect to the lambda ratio, λ (top axis) and PFT (bottom axis) for each shoe. The average roughness across shoe outsoles was used to determine the lambda ratio

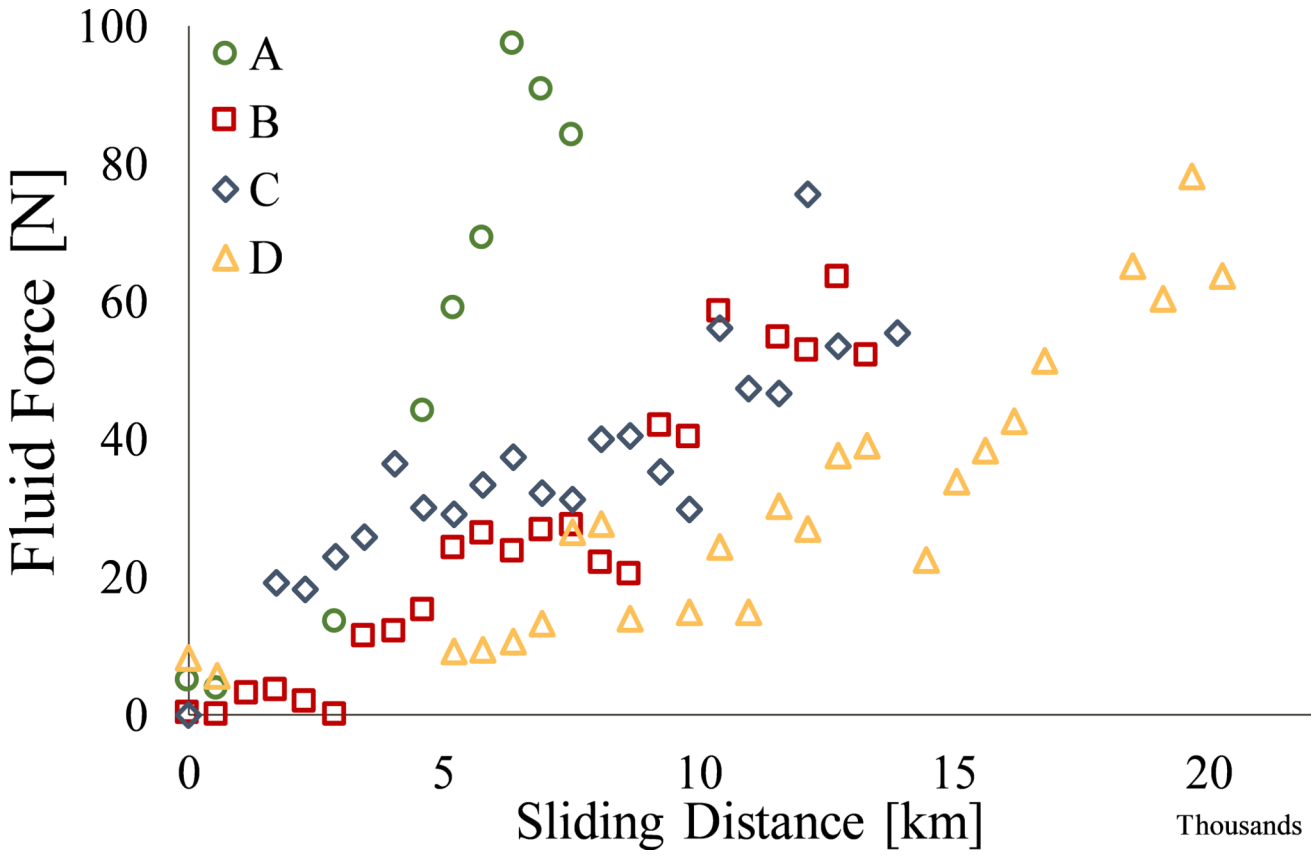

Figure 5.
Fluid force with respect to the sliding distance of the simulated wear.